Int. J. Multiphase Flow Vol. 19, No. 1, pp. 187–198, 1993
Printed in Great Britain.

0301-9322/93 $6.00 + 0.00

NUMERICAL SIMULATION AND EXPERIMENTAL INVESTIGATION OF A GAS–SOLID TWO-PHASE FLOW IN A HORIZONTAL CHANNEL

TH. FRANK, K.-P. SCHADE and D. PETRAK
Institut für Mechanik, Reichenhainer Straße 88, 9026 Chemnitz, Postfach 408, Germany

(Received 2 June 1991; in revised form 10 March 1992)

Abstract—The present paper deals with the numerical simulation of the motion of solid particles in a horizontal, two-dimensional, turbulent channel flow. The simulation is based on the Lagrangian approach, which treats the disperse phase as a number of single particles. Their trajectories are calculated by integration of the equation of motion. For the treatment of the particle–wall collision process a new approach is used, taking into consideration the influence of the wall surface roughness on the motion of the solid particles. The coefficients of dynamic friction and restitution are determined from particle–wall collision experiments. The collision of spherical particles with smooth and rough steel plates is investigated. It was found that even a very low degree of wall surface roughness has a qualitative influence on the behaviour of solid particles. Velocity and concentration profiles of the solid phase can be determined as a result of numerical simulation. The results of the numerical calculation are compared with measured particle velocity profiles and good agreement was obtained.

Key Words: numerical simulation, gas–solid flow, particles–wall interaction

1. EQUATIONS OF MOTION OF THE DISPERSE PHASE

To study the physics of confined gas–solid two-phase flow, the turbulent two-phase flow in a horizontal channel provides a classic practical example. The paper describes experimental investigations and numerical predictions of the motion of particles of mean size 65–225 μm dia in a 4.0 m long horizontal channel. In the present study the numerical prediction of a turbulent dilute two-phase flow is based on a general model for the interactions of solid particles with rough walls. The numerical results give reasonable agreement with measurements of the particle velocity and concentration.

Dilute suspensions of large particles may be treated with the Lagrangian simulation technique [see, for example, Tsuji *et al.* (1978) and Sommerfeld (1990)]. In this paper the particle phase is also treated in a Lagrangian way. The influence of the particle–particle interaction and of the particle phase on fluid phase is neglected since only dilute two-phase flow is considered. It was thus postulated that the 1/7-power law describes the axial mean gas velocity analytically. Further, in agreement with the investigations of Lee & Durst (1979) and Schönung (1983), it is possible to neglect the influence of fluid turbulence on the particle motion for the density ratio $\rho_P/\rho_F \gg 1$ and for the particle diameter range considered in this paper. In addition to the drag and gravity force, the lift force due to the particle rotation is introduced in the particle equation of motion. The term for the lift force due to the fluid velocity shear in the particle equation of motion was omitted because Saffman's (1965) expression for this force is only valid for very low particle Reynolds numbers $Re_P \ll 1$. Investigations of other authors (Hall 1988; Yamamoto *et al.* 1989) have shown that there are no reliable quantitative expressions for the mathematical description of this lift force for higher Re_P. For a spherical particle in a plane horizontal channel flow the forces, the gas velocity and the geometry are shown schematically in figure 1.

The following set of equations determines the locations and velocities of the particles:

$$\frac{d}{dt}\begin{bmatrix} u_P \\ v_P \end{bmatrix} = K_M Re_P \left(C_W(Re_P)\begin{bmatrix} u_F - u_P \\ v_F - v_P \end{bmatrix} + C_M(\xi)\begin{bmatrix} v_F - v_P \\ -(u_F - u_P) \end{bmatrix}\right) + \frac{\rho_P - \rho_F}{\rho_P}\begin{bmatrix} 0 \\ -g \end{bmatrix}, \quad [1]$$

with

$$K_M = \frac{3}{4}\frac{\nu\rho_F}{\rho_P d_P^2}, \quad Re_P = \frac{d_P v_{rel}}{\nu}, \quad \xi = \frac{1}{2}\frac{d_P \omega_P}{v_{rel}}, \quad v_{rel} = \sqrt{(u_F - u_P)^2 + (v_F - v_P)^2}, \quad [2]$$

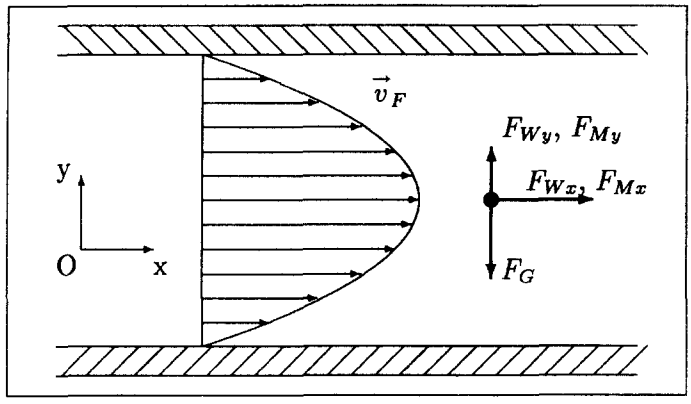

Figure 1. Composition of forces acting on a particle.

where u and v are the x- and y-components of the velocities and ρ are the densities of the fluid (F) and the particle (P), respectively; d_P is the particle diameter, ν is the fluid viscosity, g is the gravity constant and ω_P is the particle angular velocity; v_{rel} is the relative velocity between the particle and the surrounding fluid and Re_P is the particle Reynolds number.

The drag coefficient C_W as a function of Re_P is calculated using the equation of Morsi & Alexander (1972). The lift coefficient of the Magnus force C_M was assumed with (Tsuji *et al.* 1985a):

$$C_M = (0.4 \pm 0.1) \cdot \xi. \qquad [3]$$

The change in the particle angular momentum due to its interaction with the surrounding fluid was calculated using the relationship of Dennis *et al.* (1980).

In the case of large particles the particle motion is dominated by the particle–wall interactions. If it can be assumed that the particle is spherical and collides with a flat plate, the change in the particle velocity due to such a collision can be estimated by using impulsive equations with the coefficients of restitution k and dynamic friction f:

(a) for a sliding collision,

if

$$\tan\alpha_1 = \left|\frac{v_{P1}}{u_{P1}}\right| < \frac{|u_{P1} + \frac{1}{2}d_P\omega_{P1}|}{\frac{7}{2}(1+k)fu_{P1}} = \tan\alpha_{crit},$$

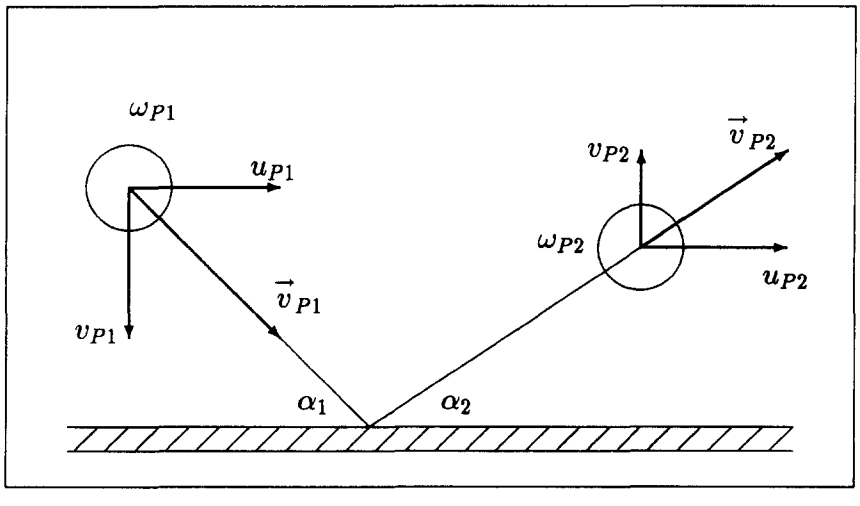

Figure 2. Collision of a spherical particle with a smooth wall surface.

then

$$u_{P2} = u_{P1} + \varepsilon(1+k)fv_{P1},$$
$$v_{P2} = -kv_{P1},$$
$$\omega_{P2} = \omega_{P1} + \varepsilon 5(1+k)f\frac{v_{P1}}{d_P},$$
$$\varepsilon = \mathrm{sgn}(u_{P1} + \tfrac{1}{2}d_P\omega_{P1}); \qquad [4]$$

and

(b) for a collision without sliding,

if

$$\tan\alpha_1 \geqslant \tan\alpha_{crit},$$

then

$$u_{P2} = u_{P1} - \frac{2}{7}\left(u_{P1} + \frac{1}{2}d_P\omega_{P1}\right),$$
$$v_{P2} = -kv_{P1},$$
$$\omega_{P2} = \omega_{P1} - \frac{5}{7}\left(\frac{2}{d_P}u_{P1} + \omega_{P1}\right); \qquad [5]$$

where the subscripts 1 and 2 are for the parameters of a particle before and after the particle–wall collision, respectively. The coefficients of restitution k and dynamic friction f have to be determined from experiments for the specific particle and wall material. Both coefficients are functions of the particle collision angle α_1.

To evaluate how far a particle can be transported by the lift force alone, simulations based on the above assumptions was carried out for different particle sizes and gas velocities. These simulations indicate that the particles soon begin to settle down at the bottom of the channel, contrary to reality. Thus, the lift force cannot be the main factor in particle behaviour, though it contributes to it.

Experimental and numerical investigations in the literature have shown that a non-spherical particle shape and even a low degree of wall surface roughness have a great effect on the behaviour of solid particles after a particle–wall collision. In this case the collision process is usually calculated by solving the impulsive equations using irregular bouncing models [see, for example, Matsumoto & Saito (1970a,b) and Tsuji *et al.* (1985b, 1989a,b)]. In the present paper a particle–wall interaction model is used which is based on a realistic geometrical model of the wall surface roughness (see figure 3). The wall surface structure is schematically described by a polygon with the elements $\{z_n, s_n\}$, where z_n and s_n are random variables distributed uniformly over $[-z_{max}, z_{max}]$ and $[\frac{1}{2}\bar{s}, \frac{3}{2}\bar{s}]$, respectively. The model parameter z_{max} and $\bar{s}$ are functions of the particle diameter d_P and of the mean values of the length scale and the amplitude of the wall surface roughness. These two roughness parameters have to be predicted by microscopic examination of wall material specimens.

The change in particle velocity due to the collision of a spherical particle with a rough wall is now determined by calculation of the particle–wall interaction of a spherical particle with the corresponding polygon element in agreement with [4] and [5]. For the coefficients k and f, functions of the particle collision angle α_1 are used.

2. EXPERIMENTAL INVESTIGATIONS OF THE PARTICLE–WALL COLLISION

In pneumatic transport the particle movement is influenced by particle–wall interactions. Especially for large particles, which are not or only slightly influenced by the fluid turbulence, these interactions are dominating for the transport process. The presented mathematical model needs the parameter of the particle–wall interaction, the coefficient of restitution and the dynamic friction coefficient.

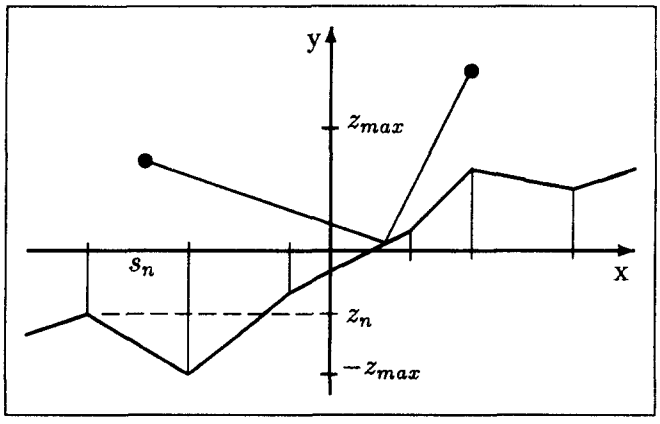

Figure 3. Geometrical model of the wall surface roughness.

In order to determine the collision parameters and to examine the described model of wall surface roughness, we investigated experimentally the collision between particles and walls with smooth and rough surfaces.

2.1. Construction of the experimental equipment

The schematic construction of the experimental equipment is shown in figure 4. The basic configuration is an angle-adjusting device. On this device, plates from several materials and with several surface structures can be mounted. With the help of a gas–particle injector particles are accelerated by an air flow and shot at the bouncing wall. Calculations and experiments showed that the influence of the gas from the particle injector on the rebound conditions of the used particles was $<1\%$. The variance of the incident angle was about 0.5°, determined from photographic particle traces.

The coefficients of restitution and dynamic friction are determined as functions of the particle collision angle, the particle translation velocity before collision, the combination of particle and wall material and the wall surface roughness. The particle velocities of the collision process were

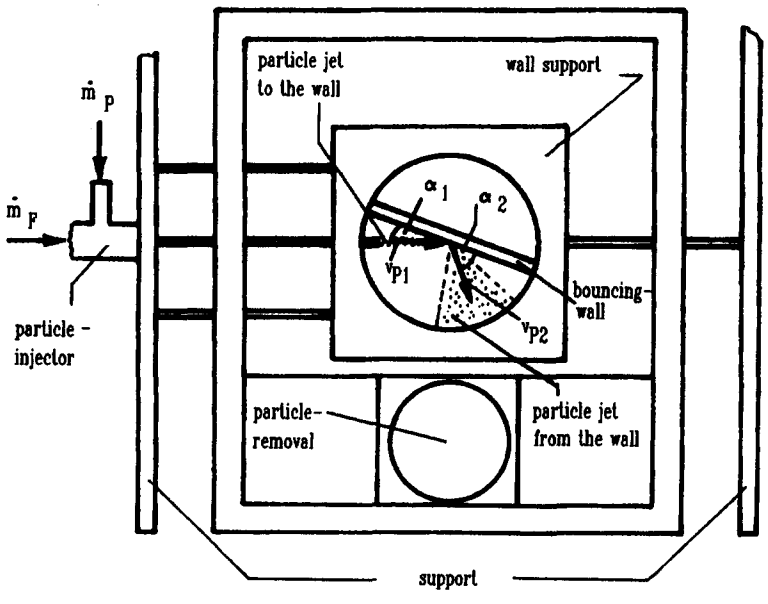

Figure 4. Experimental arrangement for the determination of coefficients of restitution and dynamic friction.

measured using two optical fibre probes and analysing their signals with a counter process (Petrak *et al.* 1989). As seen in figure 4, the particle jet from the wall is spread over a certain angle range. Therefore, it is impossible to find the correct reflection angle and the reflection velocity with only one measurement. We have constructed a special fibre probe which allows us to measure particle velocities in this angle range step by step. The construction of this probe is shown in figure 5.

The measuring system is composed of the probe with a differential-type optical fibre grating, the electronic unit for signal producing and the computer-aided signal analysis (see Petrak & Hädrich 1991). The burst signal is generated by light absorbtion or reflection by particles. We have arranged an array of 14 step-index optical fibres with a 60 μm cladding diameter and a 260 μm interval of grating lines. The probe shaft had a diameter of 6 mm and the front measuring part was 3 × 1 mm. In all measuring cases the particle diameter was smaller than the interval of grating lines. At the measuring time the sensor detected only one particle in the measuring volume. To avoid coincidence of two or more particles in the measuring volume we used a special signal analysis with a comparison of each signal burst period.

Figure 5 shows that the beginning of the fibre optical grating is arranged in the axis and the whole grating is arranged outside of the probe shaft. Therefore, it is possible to place the probe exactly at the collision point. The velocities of the reflected particle jet can be measued step by step by turning the probe around the collision point. The measuring point itself is situated nearly 2 mm above the probe surface. Therefore, the particle jet is not disturbed by the shaft of the fibre probe.

2.2. Analysis technique for measurement of the particle reflection angle and velocity

In the experimenal equipment presented here it is impossible to investigate the parameters of a single particle; only the time mean values of the particle velocity are determinable. Therefore, the collision process of the air–particle jet must be continual during the measuring time. This is realized by a constant air and particle mass flow rate.

During the measurement the special fibre probe (figure 5) is turned step by step through the reflected particle jet. The particle velocity and the number of particles per time are measured for every angle step. For example, in figure 6 the results are shown for the collision of glass particles with a mean diameter of $d_{50} = 115\ \mu$m with a plane steel wall. The variance of the particle size distribution is $\sigma = 30\ \mu$m measured with a phase Doppler anemometer. Therefore, the particle size distribution has a small influence on the results. The particle velocity before the collision was $V_{P1} = 11.66$ m/s. The angle between the particle jet and the bouncing wall was $\alpha_1 = 45°$. Figure 6 presents the ratio of the particle velocity after the collision V_{P2} to the particle velocity before the collision V_{P1} and the number of particles per time $\dot{N}$ as a function of the particle reflection angle from the wall α_2.

The particle number per time unit has a defined maximum in the range $\alpha_2 = 43° \ldots 49°$. It can be exactly determined as $\alpha_2 = 46.8°$. Under the given conditions this angle ($\alpha_2 = 46.8°$) is representative for this particle–wall collision. From this reflection angle of the particle jet we determine the corresponding value for the reflection velocity of the particles for all experiments.

The coefficients of restitution and dynamic friction can be calculated from these values using [4] of Sawatski (1961).

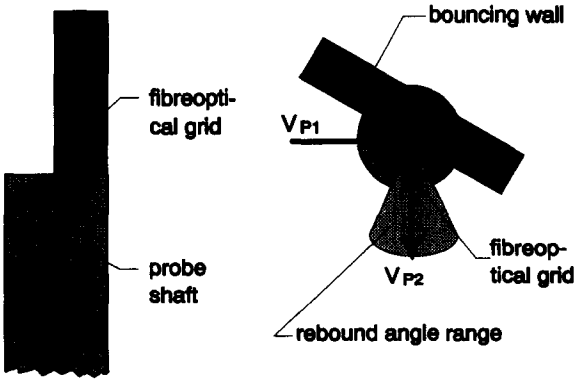

Figure 5. Construction of the special probe.

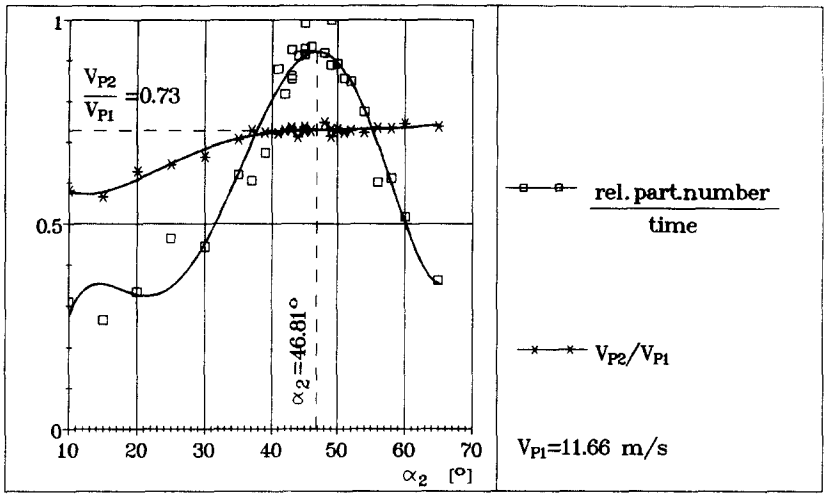

Figure 6. Impact of glass particles on a plane steel wall; $\alpha_1 = 45°$; $d_{50} = 115\,\mu$m.

2.3. *Analysis of the bouncing measurements for the smooth plate*

We investigated the collision of glass particles with a steel wall. The particles were spherical with 115 μm mean diameter and their density was 2500 kg/m^3. We carried out measurements for bouncing angles before collision of $\alpha_1 = 10°$, 30° and 45°. The velocities before bouncing V_{P1} were changed from 4 to 13 m/s for all collision angles. A defined maximum of the particle number per time unit was found for bouncing angles α_1 of 30° and 45°. For $\alpha_1 = 10°$ the measurement was more difficult. In this case the curve for the particle number per time unit was very broad and the highest values were in the angle range from 0.5° to 3°. For example, the corresponding curves for $\alpha_1 = 10°$ and for a particle velocity before collision of $V_{P1} = 5$ m/s can be seen in figure 7.

Figure 8 presents the resulting values of the coefficients of restitution as a function of V_{P1}. There is only a small difference between the k-values ($0.8 \leqslant k \leqslant 1.0$) for the bouncing angles of $\alpha_1 = 30°$ and 45°. The coefficients of restitution for $\alpha_1 = 10°$ are much smaller and about $k = 0.3$. The influence of the particle velocity before collision on the coefficients of restitution is rather small.

Figure 9 shows the corresponding dynamic friction coefficients as a function of the particle velocity before collision V_{P1} and the collision angle α_1. The value of the dynamic friction coefficients decrease with both the collision angle α_1 and the bouncing velocity V_{P1}. Our results are different from the experiments of Tabakoff and colleagues (Tabakoff & Hamed 1986; Tabakoff & Malak

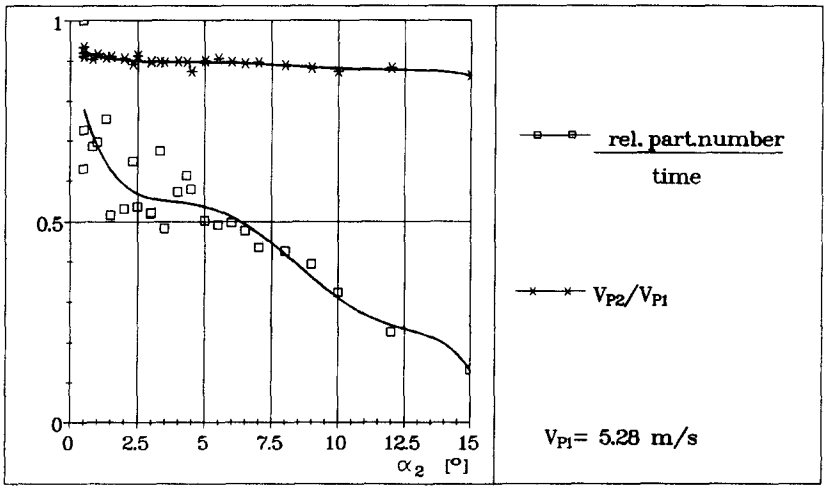

Figure 7. Particle number per time unit for bouncing angle $\alpha_1 = 10°$; $d_{50} = 115\,\mu$m.

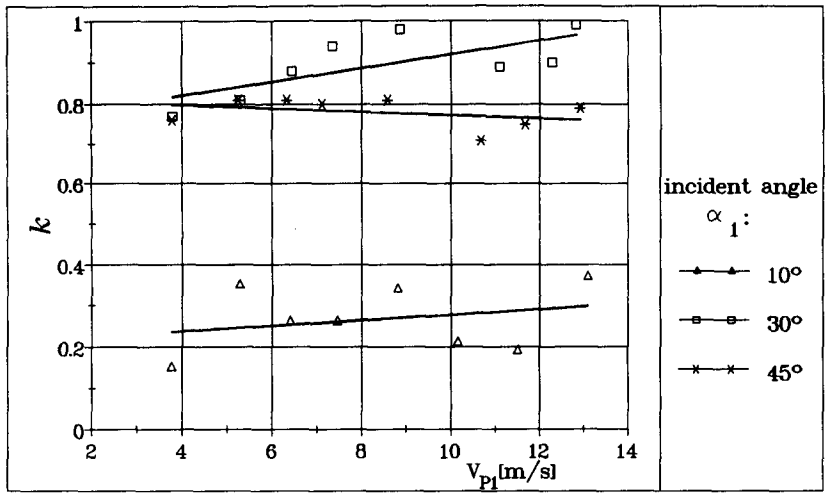

Figure 8. Coefficient of restitution; $d_{50} = 115\ \mu$m.

1987; Hamed & Tabakoff 1991). Tabakoff and colleagues describe the experimental investigation to determine the particle restitution characteristics after impacting solid targets in a particulate flow wind tunnel. The particles had a size of about 5–20 μm and a particle velocity of about 100 m/s. It was found that the values of the dynamic friction coefficients and of the coefficients of restitution decrease with the incident angle α_1. Our experiments showed that the dynamic friction coefficient decreases and the coefficient of restitution increases with the incident angle α_1.

2.4. Influence of the wall roughness

We also investigated the particle–wall collision on a wall with defined roughnesses, in order to examine the suggested geometrical model of wall surface roughness. For the collision of a spherical particle with a rough wall we expect a rebound angle α_2 which is greater than the rebound angle from a smooth wall and which depends on the kind of roughness (see also figure 10). In the rough wall experiments the particles were not deflected in the direction perpendicular to the plane of incident motion.

For these experiments we used a wall with a polished surface (roughness $R0$) and three walls with several degrees of roughness ($R1$, $R2$, $R3$). The several degrees of roughness $R1$, $R2$, $R3$ were a more "arbitrary" roughness and were generated by a planing machine. All the wall surfaces were hardened and glass particles with 115 μm mean diameter and a density of 2500 kg/m^3 were used.

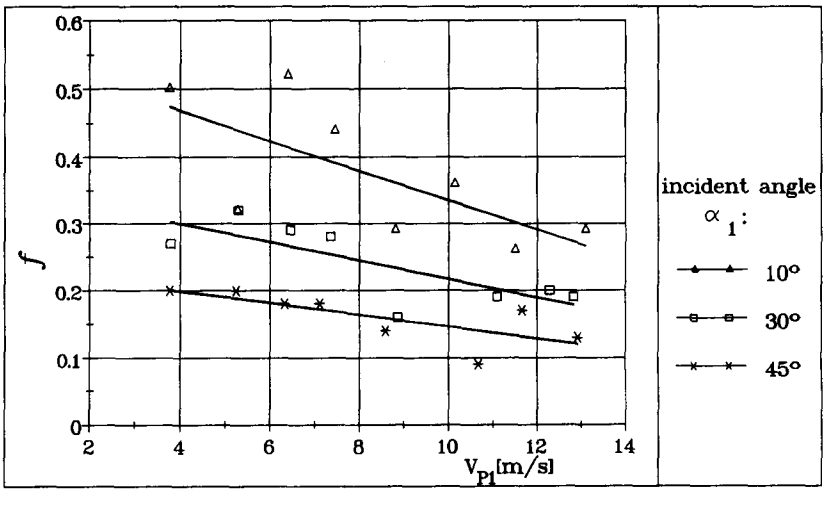

Figure 9. Coefficient of dynamic friction; $d_{50} = 115\ \mu$m.

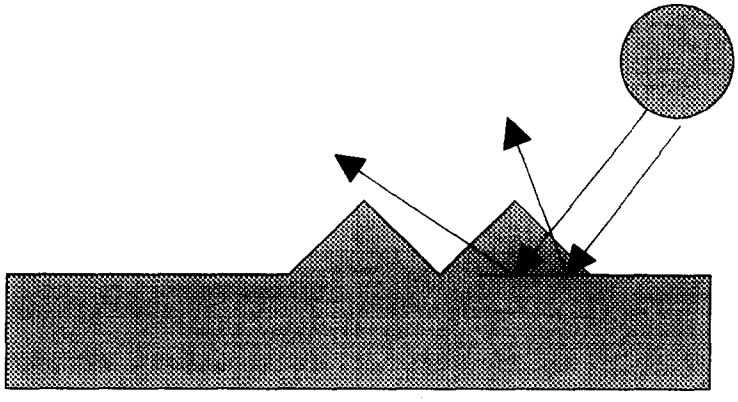

Figure 10. Principle of rebounding from a rough wall.

The bouncing angle before collision α_1 was 45° and the particle velocity before collision was varied from 4 to 13 m/s. Unfortunately, it failed to create a wall roughness of the same geometry as shown in figure 11 presents the schematic roughness profile of rough wall specimen 3.

One can see that the surface of the roughness elements is curved and so the rebound angle α_2 depends on the bouncing point of the particle (e.g. points 1–3 in figure 3 in figure 11). Both the other roughness degrees have the same shape. They differ only in the values of the length scale of the wall roughness and the roughness amplitude. The corresponding values are to be seen in figure 11. It is not possible to determine a well-defined maximum in most of the resulting distribution curves of the particle number per time as a function of the rebounding angle.

Figure 12 shows, for instance, the distribution of particle number per time for the experiments with bouncing velocity $V_{P1} = 5.2$ and 8.5 m/s and the roughness degree $R1$. In particular, an interpretation is impossible for the higher velocity.

However, most of the curves show the expected increase in the rebounding angle. Most particles will be reflected with a rebounding angle of $\alpha_2 = 65°$ (see figure 13).

All experiments described in section 2.3 show a rebounding angle of about 45° if the bouncing angle $\alpha_1 = 45°$. Figure 13 (smooth plate) shows the corresponding values for the bouncing velocity $V_{P1} = 7.1$ m/s and the bouncing angle $\alpha_1 = 45°$.

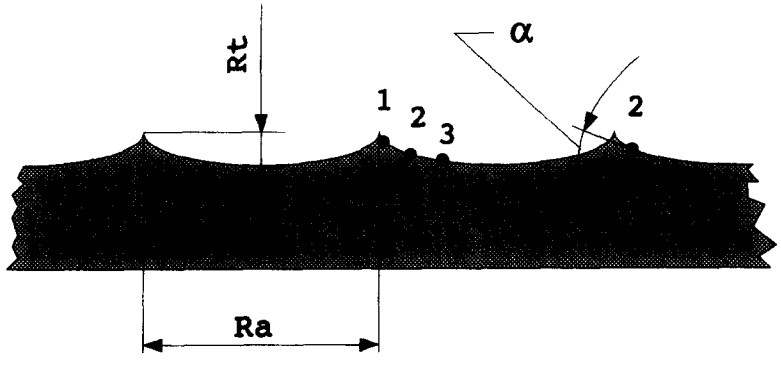

roughness	Rt (μm)	Ra (μm)	1: α = 33°
			2: α = 23°
R1	17.9	149.6	
R2	31.5	370.9	3: α = 9°
R3	43.9	588.6	

Figure 11. Surface of the rough wall.

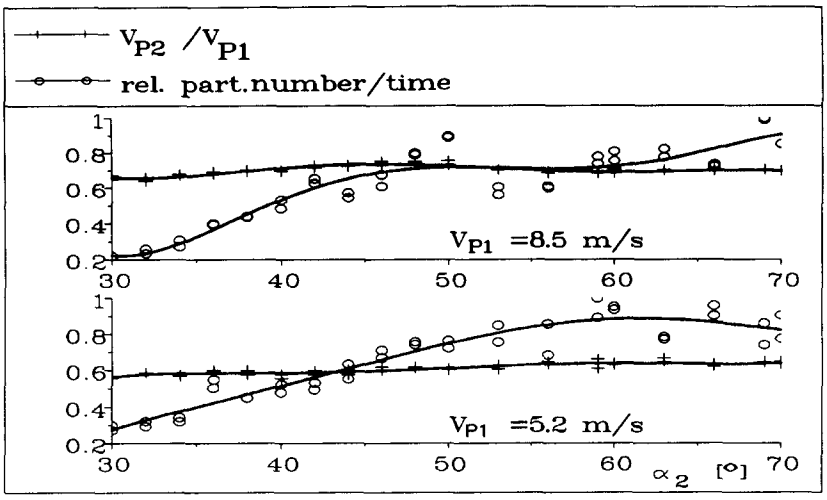

Figure 12. Particle number per time unit for wall roughness $R1$.

Surprising was the fact that the distribution of the particle number per time unit for bouncing with a polished wall shows a well-defined maximum in the range of 65° for the rebounding angle (see also figure 13, curve $R0$). A microscopic examination of the wall surface gives a description for this behaviour. Figure 14 represents the surface roughness profile of the polished plate. It is to be seen that in this case also the roughness degree is in a range which influences the particle–wall collision.

The slope of the roughness elevations of the polished plate is about 15° and, contrary to the plates with roughness degrees $R1$, $R2$ and $R3$, the peaks of the roughness profile are flattened. Therefore, the bouncing angle is well-defined and the values of the particle number per time unit have a narrow distribution near the value of the rebounding angle $\alpha_1 \sim 65°$. Summarizing the first experiments with rough walls, one can say that the suggested model of particle bouncing with rough wall surfaces is in good agreement with reality. For further investigations of the particle–wall collision process experiments with other wall roughness profiles are planned.

3. INVESTIGATION OF GAS-PARTICLE CHANNEL FLOW

The apparatus used for horizontal transport is shown schematically in figure 15. An existing pneumatic transport line was used which was made of a steel rectangular profile with a square cross

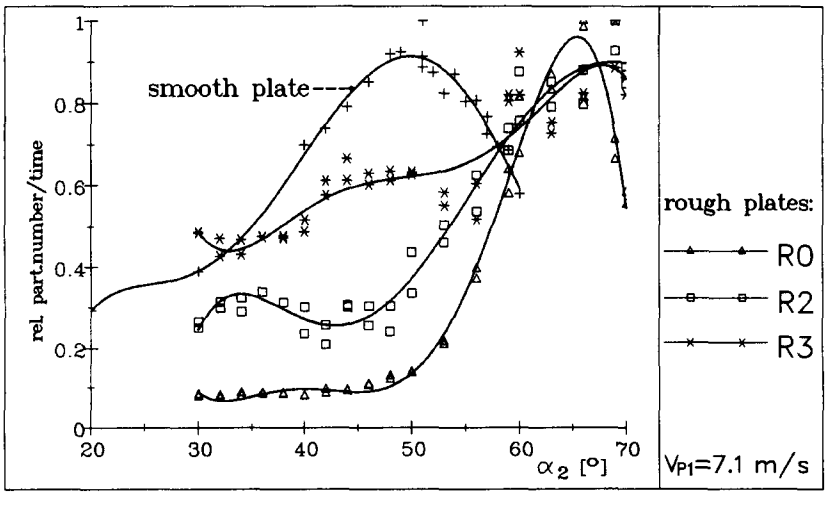

Figure 13. Particle number per time unit for several wall roughnesses.

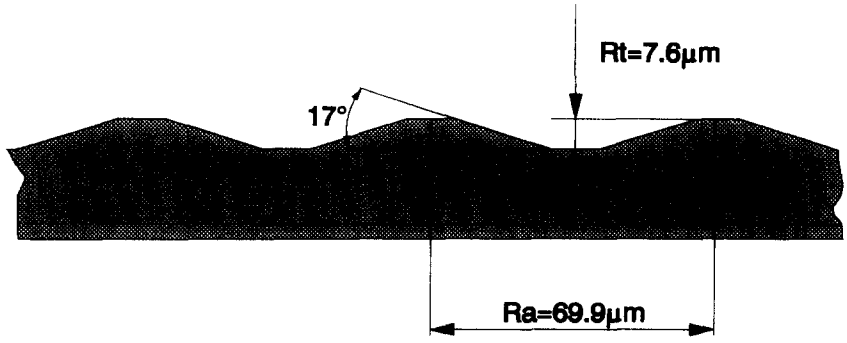

Figure 14. Roughness shape ($R0$) for the polished wall.

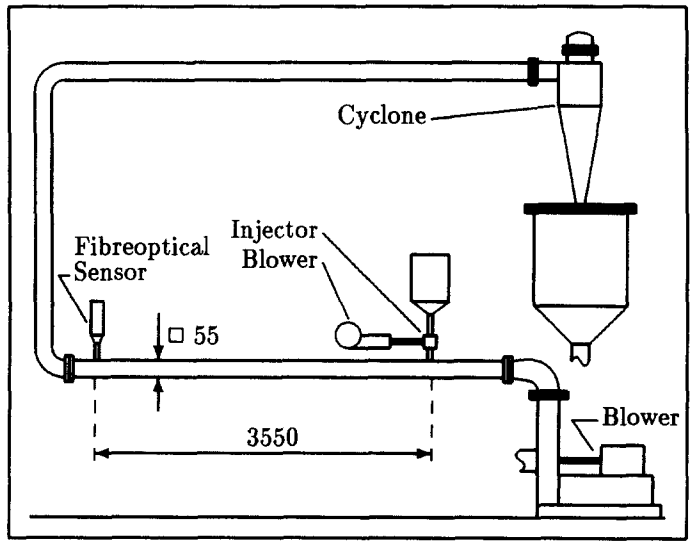

Figure 15. Test facility for horizontal pneumatic conveying.

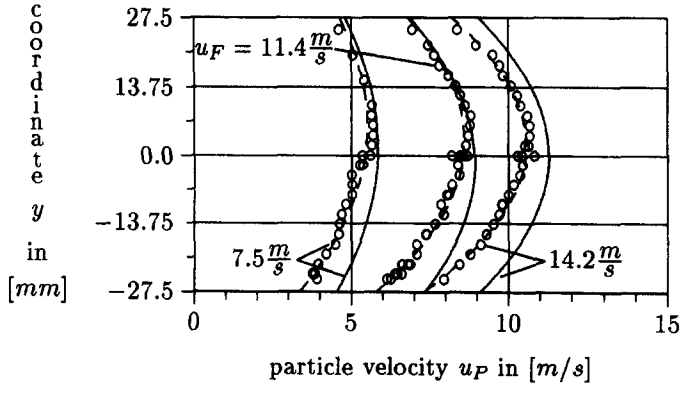

Figure 16. Comparison of the numerical simulation with the experiment for $d_{50} = 65\,\mu$m and $\sigma = 14\,\mu$m (○, experiment).

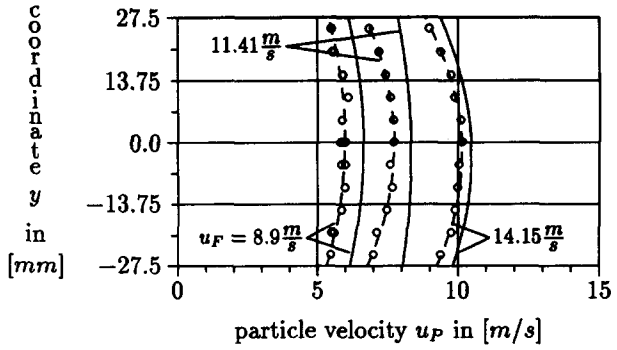

Figure 17. Comparison of the numerical simulation with the experiment for $d_{50} = 115\ \mu m$ and $\sigma = 30\ \mu m$ (○, experiment).

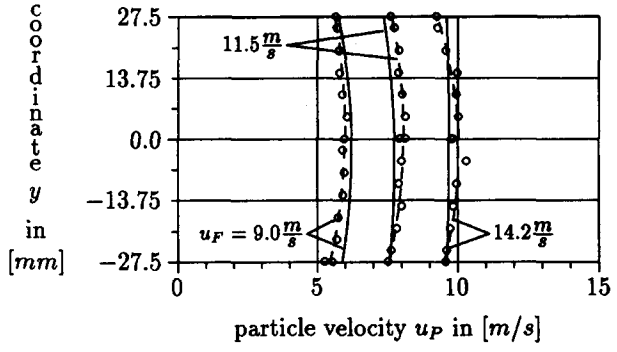

Figure 18. Comparison of the numerical simulation with the experiment for $d_{50} = 225\ \mu m$ and $\sigma = 42\ \mu m$ (○, experiment).

section of 55 × 55 mm. The test section was 6 m in length with 4 m from the particle feeding point to the measurement cross section, which was long enough for fully developed fluid flow and for full acceleration of the particles. For the improvement of this fact, a special series of experiments and numerical calculations were carried out. The particle size of the numerical simulations was the mean size of the measured particle size distributions.

Local glass particle velocities and particle concentrations were measured with fibre optical spatial filter anemometry (Petrak *et al.* 1989). The comparison of the numerical simulations with the experiments is shown, for example, in figures 16–18 for the axial particle mean velocity. The experiments and the numerical simulations were carried out for three different particle sizes and three different air velocities, measured on the channel axis.

Unfortunately, the horizontal channel used had a square cross section. So actually the fluid flow in the test section was three-dimensional and caused the particles with lower diameters to rebound from the side walls of the channel. This leads to an additional loss of kinetic energy for smaller particles and finally to lower mean particle velocities in the measurement cross section. The results of experiments with particles of $d_P = 225\ \mu m$ show that larger particles are less affected by the three-dimensional character of the fluid flow in the horizontal test section used.

4. CONCLUSIONS

An experimental method has been presented for the prediction of the coefficients of restitution and dynamic friction for the collision of spherical particles with smooth and rough wall surfaces. The influence of collision angle and particle velocity before collision has been investigated.

Using the above methods, a Lagrangian simulation has been made for a horizontal channel flow. Results have been presented about particle velocity profiles. It has been found that gas–solid flow phenomena can be predicted by the present numerical simulation using the rough wall model.

REFERENCES

DENNIS, S. C. R., SINGH, S. N. & INGHAM, D. B. 1980 The steady flow due to a rotating sphere at low and moderate Reynolds numbers. *J. Fluid Mech.* **101,** 257–279.

HALL, D. 1988 Measurements of the mean force on a particle near a boundary in turbulent flow. *J. Fluid Mech.* **187,** 451–466.

HAMED, A. & TABAKOFF, W. 1991 Experimental investigation of particle surface interactions for turbomachinery application. In *Proc. Laser-Anemometry, Cleveland, OH*, Vol. 2, pp. 775–780. ASME, New York.

LEE, S. L. & DURST, F. 1979 On the motions of particles in turbulent flows. SFB 80/TE/142, Preprint des Sonderforschungsbereichs 80, Ausbreitungs- und Transportvorgänge in Strömungen, Univ. Karlsruhe.

MATSUMOTO, S. & SAITO, S. 1970a On the mechanism of suspension of particles in horizontal pneumatic conveying: Monte Carlo simulation based on the irregular bouncing model. *J. Chem. Engng Japan* **3,** 83–92.

MATSUMOTO, S. & SAITO, S. 1970b Monte Carlo simulation of horizontal pneumatic conveying based on the rough wall model. *J. Chem. Engng Japan* **3,** 223–230.

MORSI, S. A. & ALEXANDER, A. J. 1972 An investigation of particle trajectories in two-phase flow systems. *J. Fluid Mech.* **55,** 193–208.

PETRAK, D. & HÄDRICH, TH. 1991 Laser Doppler anemometry and fibre optical spatial filter anemometry—a comparison for the multiphase flow measurement. In *Proc. Laser-Anemometry, Cleveland, OH*, Vol. 1, pp. 253–258. ASME, New York.

PETRAK, D., PRZYBILLA, E., ASTALOSCH, F., KÄMPFE, L. & HÄDRICH, TH. 1989 Fibre optical spatial filter anemometry, a local measuring technique for multiphase flows. *Tech. Messen* **56,** 72–83.

SAFFMAN, P. G. 1965 The lift on a small sphere in a slow shear flow. *J. Fluid Mech.* **22,** 385–400.

SAWATZKI, O. 1961 Über den Einfluß der Rotation und der Wandstöße auf die Flugbahnen kugliger Teilchen im Lusftstrom. Dissertation, Fakultät für Maschinenbau und Verfahrenstechnik, Univ. Karlsruhe.

SCHÖNUNG, B. 1983 Numerische Simulation teilchenbeladener vertikaler Rohströmungen. Dissertation, Fakultät für Bauingenieru- und Vermessungswesen, Univ. Karlsruhe.

SOMMERFELD, M. 1990 Numerical simulations of the particle dispersion in turbulent flow—the importance of particle lift forces and particle–wall collision models. In *Numerical Methods for Multiphase Flows*, Vol. 91. ASME, New York.

TABAKOFF, W. & HAMED, A. 1986 The dynamics of suspended solid particles in a two-stage gas turbine. *Trans. ASME Jl Turbomach.* **108,** 298–302.

TABAKOFF, W. & MALAK, M. F. 1987 Laser measurements of fly ash rebound parameters for use in trajectory calculations. *Trans. ASME Jl Turbomach.* **109,** 535–540.

TSUJI, Y., MORIKAWA, Y. & MIZUNO, O. 1985a Experimental measurement of the Magnus force on a rotating sphere at low Reynolds numbers. *Trans. ASME Jl Fluids Engng* **107,** 484–488.

TSUJI, Y., OSHIMA, T. & MORIKAWA, Y. 1985b Numerical simulation of pneumatic conveying in a horizontal pipe. *KONA—Powder Sci. Technol. Japan* **3,** 38–51.

TSUJI, Y., MORIKAWA, Y., TANAKA, T., NAKATSUKASA, N. & NAKATANI, M. 1987 Numerical simulation of gas–solid two-phase flow in a two-dimensional horizontal channel. *Int. J. Multiphase Flow.* **13,** 671–684.

TSUJI, Y., SHEN, N. Y. & MORIKAWA, Y. 1989a Numerical simulation of gas–solid flows (I)—particle to wall collision. *Technol. Rep. Osaka Univ.* **39**(1975), 233–241.

TSUJI, Y., SHEN, N. Y. & MORIKAWA, Y. 1989b Numerical simulation of gas–solid flows (II)—calculation of a two-dimensional horizontal channel flow. *Technol. Rep. Osaka Univ.* **39**(1976), 243–254.

YAMAMOTO, F., MONYA, H., KOUKAWA, M., TERANISHI, A. & TAMADA, H. 1989 A study of motion of a sphere in linear turbulent shear flow through a vertical duct. In *Proc. Int. Conf. on Mechanics of Two-phase Flows*, National Taiwan Univ., Taipei, Taiwan, pp. 45–50.